The Astrophysical Journal Letters, 977:L47 (9pp), 2024 December 20 https://doi.org/10.3847/2041-8213/ad95e8

PDS 70b Shows Stellar-like Carbon-to-oxygen Ratio

Chih-Chun Hsu[1], Jason J. Wang (王劲飞)[1,2], Geoffrey A. Blake[3], Jerry W. Xuan[4], Yapeng Zhang[4], Jean-Baptiste Ruffio[5], Katelyn Horstman[4], Julianne Cronin[1,2], Ben Sappey[5], Yinzi Xin[4], Luke Finnerty[6], Daniel Echeverri[4], Dimitri Mawet[4,7], Nemanja Jovanovic[4], Clarissa R. Do Ó[5], Ashley Baker[4], Randall Bartos[7], Benjamin Calvin[4,6], Sylvain Cetre[8], Jacques-Robert Delorme[8], Gregory W. Doppmann[8], Michael P. Fitzgerald[6], Joshua Liberman[9], Ronald A. López[6], Evan Morris[10], Jacklyn Pezzato-Rovner[4], Tobias Schofield[4], Andrew Skemer[10], J. Kent Wallace[7], and Ji Wang (王吉)[11]
[1] Center for Interdisciplinary Exploration and Research in Astrophysics (CIERA), Northwestern University, 1800 Sherman Ave., Evanston, IL 60201, USA; chsu@northwestern.edu
[2] Department of Physics and Astronomy, Northwestern University, 2145 Sheridan Rd., Evanston, IL 60208, USA
[3] Division of Geological & Planetary Sciences, California Institute of Technology, Pasadena, CA 91125, USA
[4] Department of Astronomy, California Institute of Technology, Pasadena, CA 91125, USA
[5] Department of Astronomy & Astrophysics, University of California, San Diego, La Jolla, CA 92093, USA
[6] Department of Physics & Astronomy, 430 Portola Plaza, University of California, Los Angeles, CA 90095, USA
[7] Jet Propulsion Laboratory, California Institute of Technology, 4800 Oak Grove Dr.,Pasadena, CA 91109, USA
[8] W. M. Keck Observatory, 65-1120 Mamalahoa Hwy, Kamuela, HI, USA
[9] James C. Wyant College of Optical Sciences, University of Arizona, Meinel Building 1630 E. University Blvd., Tucson, AZ 85721, USA
[10] Department of Astronomy & Astrophysics, University of California, Santa Cruz, CA 95064, USA
[11] Department of Astronomy, The Ohio State University, 100 W 18th Ave., Columbus, OH 43210, USA
Received 2024 October 30; revised 2024 November 20; accepted 2024 November 21; published 2024 December 18

Abstract

The ~5 Myr PDS 70 is the only known system with protoplanets residing in the cavity of the circumstellar disk from which they formed, ideal for studying exoplanet formation and evolution within its natal environment. Here, we report the first spin constraint and C/O measurement of PDS 70b from Keck/KPIC high-resolution spectroscopy. We detected CO (3.8σ) and H_2O (3.5σ) molecules in the PDS 70b atmosphere via cross correlation, with a combined CO and H_2O template detection significance of 4.2σ. Our forward-model fits, using BT-Settl model grids, provide an upper limit for the spin rate of PDS 70b ($<29\,\mathrm{km\,s^{-1}}$). The atmospheric retrievals constrain the PDS 70b C/O ratio to $0.28^{+0.20}_{-0.12}$ (<0.63 under 95% confidence level) and a metallicity [C/H] of $-0.2^{+0.8}_{-0.5}$ dex, consistent with that of its host star. The following scenarios can explain our measured C/O of PDS 70b in contrast with that of the gas-rich outer disk (for which C/O $\gtrsim$ 1). First, the bulk composition of PDS 70b might be dominated by dust+ice aggregates rather than disk gas. Another possible explanation is that the disk became carbon enriched *after* PDS 70b was formed, as predicted in models of disk chemical evolution and as observed in both very low-mass stars and older disk systems with JWST/MIRI. Because PDS 70b continues to accrete and its chemical evolution is not yet complete, more sophisticated modeling of the planet and the disk, and higher-quality observations of PDS 70b (and possibly PDS 70c), are necessary to validate these scenarios.

Unified Astronomy Thesaurus concepts: Exoplanet atmospheres (487); Exoplanet formation (492); High resolution spectroscopy (2096); High angular resolution (2167)

1. Introduction

Since the discovery of the first exoplanet around a Sun-like star (M. Mayor & D. Queloz 1995), >5700 exoplanets are now known.[12] Among these advances, directly imaged companions offer a unique laboratory to study exoplanet formation and evolution (B. P. Bowler 2016; T. Currie et al. 2023). These imaged planets are mostly young and warm (<500 Myr), thus bright and well separated from their host stars. Myriad protoplanetary disks have been characterized extensively in the millimeter band, but PDS 70 remains the only system that has confirmed protoplanets b and c residing in the cavity of their natal, gas-rich disk from which they formed (M. Keppler et al. 2018; A. Müller et al. 2018; S. Y. Haffert et al. 2019),[13] serving as a unique opportunity to study exoplanet formation and evolution in situ.

PDS 70 A is a K7 T Tauri star in the Upper Centaurus Lupus association at 112 pc (M. J. Pecaut & E. E. Mamajek 2016; M. Keppler et al. 2018; Gaia Collaboration et al. 2023), with a slightly subsolar metallicity ([Fe/H] = -0.11 ± 0.1; M. Steinmetz et al. 2020b), a C/O ratio of 0.44 ± 0.19 (A. J. Cridland et al. 2023), and an age of 5.4 ± 1.0 Myr (P. Riaud et al. 2006; M. J. Pecaut & E. E. Mamajek 2016).[14] PDS 70b has a mass of 2–4 $M_{\rm Jup}$, a semimajor axis of $20.8^{+0.6}_{-0.7}$ au, and a nonzero orbital eccentricity of 0.17 ± 0.06; while PDS 70 c has a mass of 1–3 $M_{\rm Jup}$ with a circular orbit (eccentricity $0.037^{+0.041}_{-0.025}$) at $34.3^{+2.2}_{-1.8}$ au (J. J. Wang et al. 2020, 2021c). PDS 70b and c

[12] NASA Exoplanet Archive compilation on 2024 October 7; https://exoplanetarchive.ipac.caltech.edu/.

[13] AB Aur b is a confirmed protoplanet with its disk (T. Currie et al. 2022). See also other candidates summarized in T. Currie et al. (2023).

[14] We note that PDS 70 A might be a member in the subgroup ν Cen of the Upper Centaurus Lupus, with reported ages between ~9 and 16 Myr (S. Ratzenböck et al. 2023a, 2023b), while most disk lifetimes are less than 10 Myr (S. Pfalzner & F. Dincer 2024).

Table 1
PDS 70 A and B Properties

Property (unit)	Value	References
	PDS 70 A	
R.A. (J2000)	14:08:10.15	(1)
decl.. (J2000)	−41:23:52.57	(1)
μ_α (mas yr^{-1})	−29.70 ± 0.02	(1)
μ_δ (mas yr^{-1})	−24.04 ± 0.02	(1)
Mass ($M_\odot$)	0.88 ± 0.02	(2)
Age (Myr)	~5	(3)
SpT	K7IVe	(4)
Gaia G	11.606 ± 0.004	(1)
$J_{\rm MKO}$ (mag)	9.55 ± 0.02	(5)
$H_{\rm MKO}$ (mag)	8.82 ± 0.04	(5)
$K_{\rm S,MKO}$ (mag)	8.54 ± 0.02	(5)
π (mas)	8.898 ± 0.019	(1)
distance (pc)	112.4 ± 0.2	(1)
RV (km s^{-1})[a]	$6.65^{+0.14}_{-0.22}$	(9)
$v \sin i$ (km s^{-1})	$17.3^{+0.4}_{-0.3}$	(9)
[Fe/H] (dex)	−0.11 ± 0.1	(6)
C/O	0.44 ± 0.19	(7)
	PDS 70b	
Mass ($M_{\rm Jup}$)	2–4	(7)
Radius ($R_{\rm Jup}$)	$2.7^{+0.4}_{-0.3}$	(8)
a (au)[b]	$20.8^{+0.6}_{-0.7}$	(2)
e [b]	0.17 ± 0.06	(2)
i (deg)[b]	$130.5^{+2.5}_{-2.4}$	(2)
$T_{\rm eff}$ (K)	1204^{+52}_{-53}	(8)
L' (mag)	14.64 ± 0.18	(8)
$v \sin i$ (km s^{-1})	<29[c]	(9)
RV (km s^{-1})[a]	$-1.7^{+3.4}_{-5.2}$	(9)
[C/H] (dex)	$-0.2^{+0.8}_{-0.5}$	(9)
C/O	$0.28^{+0.20}_{-0.12}$	(9)

Notes.
[a] Barycentric RV on MJD 60453.27578.
[b] Dynamically stable solutions in J. J. Wang et al. (2021c).
[c] Upper limit at 95% confidence level.
References. (1) Gaia Collaboration et al. (2023); (2) J. J. Wang et al. (2021c); (3) A. Müller et al. (2018); (4) M. J. Pecaut & E. E. Mamajek (2016); (5) R. M. Cutri et al. (2003); (6) M. Steinmetz et al. (2020b); (7) A. J. Cridland et al. (2023); (8) J. J. Wang et al. (2020); (9) This work.

show clear signs of Hα (S. Y. Haffert et al. 2019), indicative of ongoing accretion, but no detections of Hβ were reported in J. Hashimoto et al. (2020).

The PDS 70 outer disk has a gas-phase C/O ratio $\gtrsim 1$ as inferred from Atacama Large Millimeter/submillimeter Array (ALMA) spectroscopy (S. Facchini et al. 2021; A. J. Cridland et al. 2023; C. J. Law et al. 2024), and the PDS 70 inner disk was detected in H_2O and CO_2 with JWST/MIRI (G. Perotti et al. 2023). Both PDS 70b and c lie within the CO ice line (at 56–85 au; A. J. Cridland et al. 2023; C. J. Law et al. 2024). The measurements of the C/O ratio of PDS 70b and c are crucial for constraining the formation and evolution of the planetary system, but no clear molecular detections have been reported prior to this work, despite attempts such as the one using the SINFONI integral field spectrograph (R ~ 5000) at the Very Large Telescope (VLT; G. Cugno et al. 2021). The PDS 70 A and b properties relevant to this work are summarized in Table 1.

In this Letter, we report the first abundance measurement of the protoplanet PDS 70b using atmospheric molecular line detections of CO and H_2O from Keck/Keck Planet Imager and Characterizer (KPIC) high-resolution spectroscopy. In Section 2, we describe our KPIC observation and data reduction. Section 3 presents our detection of CO and H_2O, while Sections 4 and 5 show our forward-modeling results using a self-consistent modeling and retrieval framework, respectively. In Section 6, we discuss possible interpretations of our measured C/O of PDS 70b with the host star and disk measurements in the literature. We summarize our findings in Section 7.

2. Observations and Data Reduction

The KPIC connects the Keck II Telescope's adaptive optics system to the infrared high-resolution spectrograph NIRSPEC (I. S. McLean et al. 1998, 2000; E. C. Martin et al. 2018) using single-mode fibers (D. Mawet et al. 2016, 2017; J.-R. Delorme et al. 2021), enabling diffraction-limited high-resolution spectroscopy (R ~ 35,000). KPIC underwent a series of upgrades in 2024 April (D. Echeverri et al. 2024; K. A. Horstman et al. 2024; N. Jovanovic et al. 2024, submitted).

We observed PDS 70b on 2024 May 23 (UT) under clear and stable weather conditions, with a natural seeing of 0.″65. We used KPIC fibers 2 and 4 (out of the four KPIC fibers). The total exposure time on PDS 70b was limited to 140 minutes (fourteen 600 s exposures) due to the source decl. and the Nasmyth platform limit of the Keck II telescope. KPIC observations require an orbital prediction of the planet to offset from the host star, and we used the astrometry solutions in J. J. Wang et al. (2021c) and `whereistheplanets` (J. J. Wang et al. 2021a)[15] and offset to the separation of 148.76 mas and position angle of 128.28 mas relative to the host star PDS 70 A during our observations. We also observed PDS 70 A and used on-axis star spectra as an empirical star template to model the starlight contribution injected into the fiber pointed at the planet. The exposure time on PDS 70 A was taken as six 180 s exposures using KPIC fibers 2 and 4, for a total of 18 minutes, roughly before and after a set of 40–60 minute exposures on PDS 70b. For the spectral trace identifications and telluric calibrator, we used the A0V star HD 118214 (A. Cowley et al. 1969), with two exposures of 30 s for each fiber. For the wavelength calibration, we used early M giant star (C-R4IIIb; P. C. Keenan 1993) HIP 62944, with two exposures of 30 s for each fiber. HIP 62944 has narrow spectral lines and telluric lines that enable precise wavelength calibration.

Our KPIC data were reduced using the `KPIC Data Reduction Pipeline`,[16] with the procedures detailed in J. J. Wang et al. (2021b) and C.-C. Hsu et al. (2024b), using background subtraction and optimal source extraction (K. Horne 1986). The PDS 70 A and PDS 70b spectra were background subtracted using the thermal background frames of the corresponding integration times (180 and 600 s for PDS 70 A and b, respectively).

3. Cross-correlation Function Detection

Our detection of PDS 70b uses the forward-modeling cross-correlation function (CCF) technique. We refer readers to

[15] http://whereistheplanet.com/
[16] https://github.com/kpicteam/kpic_pipeline

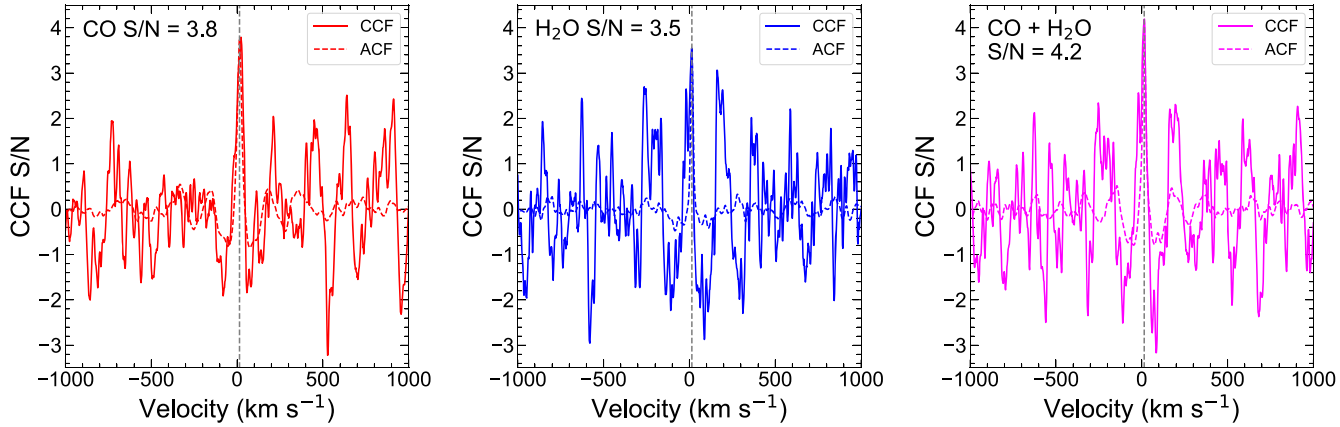

Figure 1. Cross-correlation functions (CCFs) of our PDS 70b KPIC spectra against the molecular templates derived from the Sonora Bobcat models. Left: CCF (red solid line) of our KPIC spectra for the CO molecular templates. The stellar barycentric–included RV is depicted by the gray vertical dashed line. The auto-correlation function (ACF) of the CO molecular templates, normalized to the peak of CCF, is plotted as a dashed red line. The ACF serves as a guide to detections of given molecular templates. Middle: same as the left panel for the H_2O molecular templates in blue. Right: same as the upper panel for the CO + H_2O molecular templates in magenta.

J. J. Wang et al. (2021b), J. W. Xuan et al. (2022), and C.-C. Hsu et al. (2024b) for the formulation and implementation of our methods.

In short, we jointly fit for the host star contribution, the planet template with various combinations of molecules, and the telluric and instrument response using the least-squares-fit-based CCF. The CCF signal of a given velocity shift was obtained by optimizing the amplitude of the host star contribution (from the observed on-axis star spectra) and the planet templates. Our planet templates including only CO or H_2O along with combined CO + H_2O opacities are derived from Sonora Bobcat models (M. Marley et al. 2018; M. S. Marley et al. 2021) at effective $T_{\rm eff} = 1200$ K and a surface gravity of $\log g = 4.0$ cgs dex (J. J. Wang et al. 2021b), consistent with the PDS 70b parameters derived in J. J. Wang et al. (2021c). We ran the velocity from -1000 to $+1000$ km s^{-1} and used the last ± 800 km s^{-1} CCF wings to compute the noise and estimate the signal-to-noise ratio (SNR). We found detections of CO (CCF SNR ~ 3.8), H_2O (CCF SNR ~3.5), and CO + H_2O (CCF SNR ~ 4.2) in our CCF curves, as shown in Figure 1. We further constrain the physical parameters of PDS 70b in Sections 4 and 5.

4. Bulk Parameters of PDS 70 A and B

4.1. PDS 70 A

If distinct, fits of the radial velocity (RV) of PDS 70 A and 70 b on the same night can help us validate our protoplanet detection. We forward-modeled NIRSPEC order 33 (2.29–2.34 μm) of our PDS 70 A spectra using the `SMART` package (C.-C. Hsu et al. 2021a, 2021b), with the procedures detailed in C.-C. Hsu et al. (2021a, 2023).

The forward method fits the stellar spectra using the BT-Settl CIFIST models (I. Baraffe et al. 2015), along with a telluric model as a function of air mass and precipitable water vapor (S. Moehler et al. 2014). The best-fit parameters were derived using the Markov Chain Monte Carlo (MCMC) package `emcee` (D. Foreman-Mackey et al. 2013). We incorporated a fringe model determined outside of MCMC, using a formulation similar to B. Cale et al. (2019; see also K. A. Horstman et al. 2024; W. Xuan et al. 2024b). There are nine parameters in our MCMC forward-model fit: effective temperature ($T_{\rm eff}$), surface gravity ($\log g$), RV, projected rotational velocity ($v \sin i$), air mass, precipitable water vapor, and three nuisance parameters (flux and wavelength offsets, and a noise inflation scale factor). We used 100 chains and 10,000 steps, with a burn-in of the first 2000 steps. Convergence occurred within the first 1000 steps verified by visual inspection of the chain evolutions.

Our best-fit values are $T_{\rm eff} = 3849^{+108}_{-39}$ K, $\log g = 5.20 \pm 0.04$ cm s^{-2} dex, $v \sin i = 17.3^{+0.4}_{-0.3}$ km s^{-1}, and (barycentric velocity–corrected) RV $= 6.65^{+0.14}_{-0.22}$ km s^{-1}, while our measured $v \sin i$ is consistent with the literature measurement of 17.16 ± 0.16 km s^{-1} (T. Thanathibodee et al. 2020; C. Swastik et al. 2021; B. P. Bowler et al. 2023). Our RV is consistent with lower-resolution spectroscopic measurements such as RAVE (4 ± 7 km s^{-1}; M. Steinmetz et al. 2020a), Gaia (3.1 ± 1.4 km s^{-1}; Gaia Collaboration et al. 2018), and HARPS RV $= +6.0 \pm 1.5$ km s^{-1} (T. Thanathibodee et al. 2020). Our derived RV of PDS 70 A is also consistent with the optimal RV of 4.8 km s^{-1} for belonging to the ν Cen membership reported in S. Ratzenböck et al. (2023a, 2023b), while their RV scatters in the subgroup are typically a few km s^{-1}. When determined solely through high-resolution spectroscopy over narrow wavelength ranges, $T_{\rm eff}$ and $\log g$ measurements can have significant uncertainties. We therefore stress that our RV and $v \sin i$ constraints, which are our targeted physical parameters in this work, are largely insensitive to the true values of $T_{\rm eff}$ and $\log g$ (see discussions and justifications in C.-C. Hsu et al. 2021a, 2024a and C. A. Theissen et al. 2022).

4.2. PDS 70b

To determine the atmospheric parameters of PDS 70b, we forward-modeled the observed KPIC spectra of PDS 70b by simultaneously fitting stellar, which is the diffracted starlight that leaks into the fiber pointed at the planet, and planet flux contributions. The fitting procedures are detailed in C.-C. Hsu et al. (2024b). For the wavelength range of our analysis, we used the NIRSpec orders 31–33 (2.29–2.49 μm), as these contain CO, H_2O, and CH_4 features and provided the best wavelength calibration. We used the on-axis KPIC spectra of PDS 70 A to serve as an empirical template and the BT-Settl CIFIST model grids (I. Baraffe et al. 2015) for the planet model. In short, we fitted 17 parameters in total, including $T_{\rm eff}$,

Table 2
Forward-modeling Priors and Results

Description	Symbol (unit)	Priors[a]	Results[b]
BT-Settl Fits			
Effective Temperature	$T_{\rm eff}$ (K)	$\mathcal{U}(800, 1800)$	1103^{+134}_{-75}
Surface Gravity	$\log g$ (dex cm s^{-2})	$\mathcal{U}(3.5, 5.5)$	$4.7^{+0.5}_{-0.6}$
Projected Rotational Velocity	$v \sin i$ (km s^{-1})	$\mathcal{U}(0, 100)$	9^{+9}_{-7}[c]
Radial Velocity	RV (km s^{-1})	$\mathcal{U}(-100, 100)$	$-1.7^{+2.3}_{-4.6}$[d]
Planet Flux	Planet Flux (DN)	$\mathcal{U}(0, 160)$	$3.6^{+1.2}_{-1.1}$
Speckle Flux for Fiber 2[e]	Speckle Flux (DN)	$\mathcal{U}(-50, 200)$	120 ± 2
Speckle Flux for Fiber 4[e]	Speckle Flux (DN)	$\mathcal{U}(-50, 200)$	110 ± 2
Scale Term for LSF[e]	LSF σ	$\mathcal{U}(1.0, 1.2)$	$1.11^{+0.06}_{-0.07}$
Error Jitter[e]	Error Jitter (DN)	$\mathcal{U}(0.1, 30.0)$	2.23 ± 0.02
Retrieval Fits			
Effective Temperature[f,g]	$T_{\rm eff}$ (K)	1100	⋯
Surface Gravity[f,g]	$\log g$ (dex cm s^{-2})	4.5	⋯
Projected Rotational Velocity[g]	$v \sin i$ (km s^{-1})	0	⋯
Radial Velocity	RV (km s^{-1})	$\mathcal{U}(-15, 15)$	$-4.4^{+2.0}_{-2.1}$[d]
Carbon/Oxygen	C/O	$\mathcal{U}(0.1, 1.6)$	$0.28^{+0.20}_{-0.12}$
Metallicity	[C/H]	$\mathcal{U}(-1.5, 1.5)$	$-0.2^{+0.8}_{-0.5}$
Quench Pressure	$\log P_{\rm quench}$ (bar)	$\mathcal{U}(-4, 3)$	$1.6^{+0.9}_{-0.8}$
Planet Flux	Planet Flux (DN)	$\mathcal{U}(0, 160)$	$2.7^{+1.2}_{-1.0}$
Speckle Flux for Fiber 2[e]	Speckle Flux (DN)	$\mathcal{U}(-50, 200)$	120 ± 2
Speckle Flux for Fiber 4[e]	Speckle Flux (DN)	$\mathcal{U}(-50, 200)$	111 ± 2
Scale Term for LSF[e]	LSF σ	$\mathcal{U}(1.0, 1.2)$	1.10 ± 0.07
Error Jitter[e]	Error Jitter (DN)	$\mathcal{U}(0.1, 30.0)$	2.22 ± 0.02

Notes.
[a] $\mathcal{U}$ represents uniform priors with the lower and upper bounds in the parentheses.
[b] The uncertainties are reported as the 16th and 84th percentiles.
[c] Our $v \sin i$ measurement is consistent with a nondetection (<29 km s^{-1} at 95% confidence interval). See Section 4.2 for details.
[d] Our reported RV has been corrected with the barycentric velocity during the observation (−7.59 km s^{-1}).
[e] There are three parameters used to fit in orders 31–33. We show only order 33 as an illustration here.
[f] We used the Sonora Bobcat pressure–temperature profile (M. S. Marley et al. 2021).
[g] Fixed parameters determined in our BT-Settl results. See Sections 4.2 and 5 for details.
[h] Our range of C/O priors is limited from 0.1 to 1.6 by the chemistry in `petitRADTRANS`(P. Mollière et al. 2020).

$\log g$, RV, $v \sin i$, planet flux in counts (5 parameters), and stellar contribution along with nuisance parameters (12 parameters). Each order has two star-flux terms in counts (for fibers 2 and 4), one line spread function scale factor, and one noise jitter term. The best-fit parameters are derived using the nested sampling method `dynesty` (J. S. Speagle 2020) with 1000 live points. The normal χ^2-based log-likelihood is defined in C.-C. Hsu et al. (2024b). Our priors and resulting parameters are summarized in Table 2.

Figure 2 shows the KPIC spectra of PDS 70b as well as its best-fit forward model. The posterior probability distributions are shown in Figure 3. Our best-fit values are $T_{\rm eff} = 1003^{+134}_{-75}$ K, $\log g = 4.7^{+0.5}_{-0.6}$ cm s^{-2} dex, $v \sin i = 9^{+9}_{-7}$ km s^{-1} (consistent with a nondetection of spin; see discussions below), and the barycentric-corrected RV $= -1.7^{+2.3}_{-4.6}$ km s^{-1}. Our measured PDS 70 A RV is $6.65^{+0.14}_{-0.22}$ km s^{-1} (Section 4.1) which differs by 3.6σ from PDS 70b (i.e., $\Delta{\rm RV} = {\rm RV}_{\rm planet} - {\rm RV}_{\rm star} = -8.4^{+2.3}_{-4.6}$ km s^{-1} on MJD 60453.27578). However, the RV difference is too large compared to the predicted RV amplitude of PDS 70b based on orbital solutions in J. J. Wang et al. (2021c; ~2.2 km s^{-1} at the epoch of our observation). We attributed the discrepancy to the systematics and added 2.5 km s^{-1} as our systematic uncertainty based on the RV analysis in K. Horstman et al. (2023), with our resulting RV $= -1.7^{+3.4}_{-5.2}$ km s^{-1} for PDS 70b. Our $v \sin i = 9^{+9}_{-7}$ km s^{-1} (<29 km s^{-1} at 95% confidence level) with a posterior probability distribution peak near 0, so we ran another forward-model fit with the $v \sin i$ set as 0. We found that our result highly favors the nondetection of spin in our KPIC spectra of PDS 70b, with $\log_{10}$ Bayes factor = 510.7 (decisive; H. Jeffreys 1961) and $\Delta\chi^2 = 779$. The nondetection of spin is expected as PDS 70b is still accreting and has not yet undergone the contraction and spin-up phase (M. L. Bryan et al. 2020; C.-C. Hsu et al. 2024a). Our KPIC spectra of PDS 70b did not show the Brackett γ line emission (~2.166 μm), similar to previous nondetections reported in V. Christiaens et al. (2019) and J. J. Wang et al. (2021c). While our derived $T_{\rm eff}$ and $\log g$ values are consistent with literature measurements using photometry (J. J. Wang et al. 2021c), we again stress the limitations of high-resolution spectroscopy in measuring these parameters for low-temperature objects (C.-C. Hsu et al. 2021a, 2024a). To examine whether clouds are necessary to fit the data better, we used the Sonora Bobcat (cloudless) model grids (M. S. Marley et al. 2021) and found a worse fit compared to our BT-Settl result ($\log_{10}$ Bayes factor = 0.7, which is substantial following H. Jeffreys 1961 and equivalent to 2.4σ significance following B. Benneke & S. Seager 2013).

To further validate our detection of PDS 70b if there is indeed planet signal in our data, we ran a stellar model only fit to our KPIC PDS 70b spectra. We found that such a star-only model is highly disfavored compared to our combined planet and star model, with $\log_{10}$ Bayes factor = 344.9, considered decisive (H. Jeffreys 1961). The $\Delta\chi^2$ of 772 further supports our detection of PDS 70b.

5. Retrieval Analysis

We constrained the C/O ratio and metallicity [C/H] from our KPIC spectra of PDS 70b, using the `petitRADTRANS` package (P. Molliére et al. 2019, 2020). Our method follows the retrieval framework in J. W. Xuan et al. (2022) and C.-C. Hsu et al. (2024b). Since our KPIC spectra of PDS 70b signals are still relatively noisy (Section 3), we constrained our retrieval model with parameters determined in the self-consistent BT-Settl model grids in Section 4.2. We used the Sonora pressure–temperature profile at $T_{\rm eff} = 1100$ K and $\log g = 4.5$ cm s^{-2}, and $v \sin i$ at 0 km s^{-1} was fixed (Section 4.2) with a cloudless model. We also restricted our RV priors between ± 15 km s^{-1} to avoid RVs stuck in the unphysical

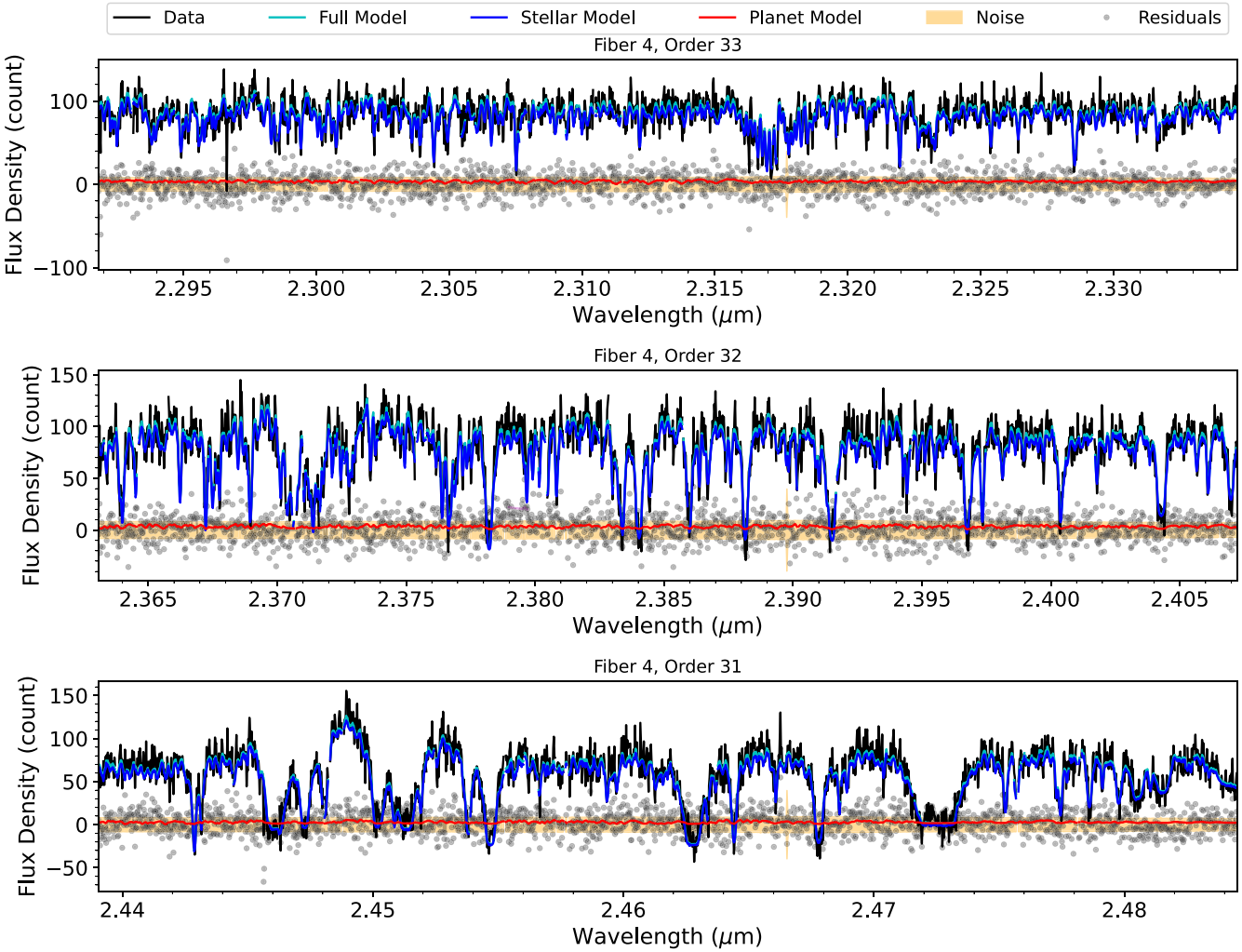

Figure 2. KPIC spectrum of PDS 70b and its best-fit forward model using the BT-Settl model grids. The spectra were taken on 2024 May 23 (UT). Orders 31–33 on fiber 4 are shown in black lines. The full forward model, with the stellar speckle and planet fluxes, is in cyan lines. The stellar model, directly from the observed on-axis KPIC spectrum of PDS 70 A, is shown in blue lines. The planet model, including the best-fit BT-Settl model with the observed telluric profile, is illustrated in red lines. The residual (data—full forward model) is depicted in gray dots, and data noise is shown in the orange shaded region.

parameter space. We adopted the chemical disequilibrium model parameterized by the quench pressure $P_{\rm quench}$ in Mollière et al. (2020). Our full forward retrieval model has 17 parameters in total, including RV, C/O, [C/H], $\log P_{\rm quench}$, planet flux counts, and the 12 nuisance parameters defined in Section 4.2.

For the molecular species, we used the line-by-line approach, including all CO isotopologues ("CO_all_iso"), the principal H_2O isotopologue ("H2O_main_iso") from the HITEMP database (L. S. Rothman et al. 2010), and the parent CH_4 species ("CH4_hargreaves_main_iso") from R. J. Hargreaves et al. (2020). We also included Rayleigh scattering from hydrogen and helium (A. Dalgarno & D. A. Williams 1962; Y. M. Chan & A. Dalgarno 1965) and continuum collision-induced absorption opacities for H_2–H_2 and H_2–He (D. F. Gray 2008). To expedite the computation, the resolution of the opacities ($R = 10^6$) was downsampled by a factor of 4 (i.e., to $R = 2.5 \times 10^5$).

We again used the nested sampling method with 1000 live points (as in Section 4.2) to derive our best-fit model. The fixed parameters, priors, and best-fit parameters are summarized in Table 2. Figure 3 shows the posteriors for RV, C/O, and [C/H] from our best-fit forward retrieval model. Our best-fit values are $\mathrm{C/O} = 0.28^{+0.20}_{-0.12}$ ($\lesssim$0.63 at 95% confidence level) and $[\mathrm{C/H}] = -0.2^{+0.8}_{-0.5}$ dex, which are consistent with solar and the host star metallicity. Our best-fit $\mathrm{RV} = -4.4^{+2.0}_{-2.1}\,\mathrm{km\,s^{-1}}$ is consistent with our RV derived in our BT-Settl fit.

6. Discussion

One route to constraining the formation history of PDS 70b is to place our measured C/O ratio and metallicity for the protoplanet (C/O $\lesssim$ 0.63; Section 5) in the context of that of the host star PDS 70 A (C/O ~ 0.44; A. J. Cridland et al. 2023) and the outer gas disk (C/O $\gtrsim$ 1; S. Facchini et al. 2021; A. J. Cridland et al. 2023; C. J. Law et al. 2024). We note that the ALMA gas disk C/O measurements in S. Facchini et al. (2021), A. J. Cridland et al. (2023), and C. J. Law et al. (2024) only probe the gas-phase C and O reservoirs, typically at large-scale heights in the disk, whereas the solids are often located near the disk midplane and with compositions that are impossible to constrain with the current facilities. Were the metallicity of PDS 70b substellar but with a high C/O ratio, this would likely indicate that the bulk of the accretion onto PDS 70b came from the gas phase of the disk within its Hill radius (K. I. Öberg et al. 2011). However, our measured C/O

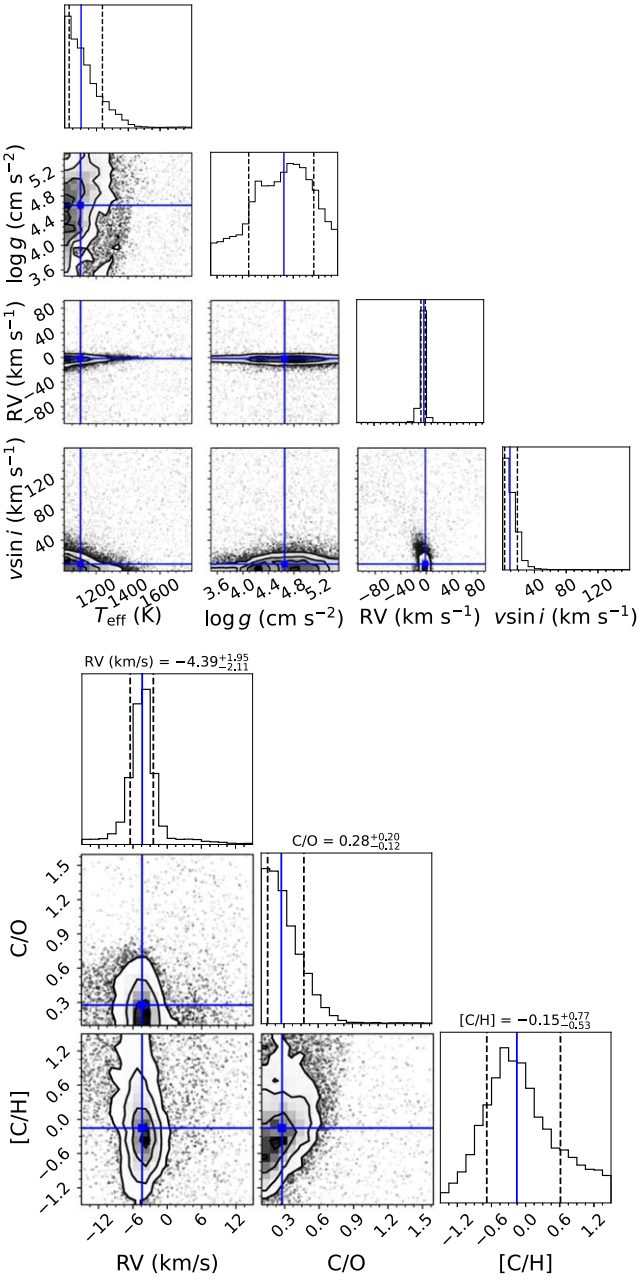

Figure 3. Top: posteriors of the derived physical parameters of PDS 70b using the BT-Settl models, including effective temperature, surface gravity, and projected rotational and radial velocities. See Section 4.2 for details. Bottom: the posteriors of RV, C/O ratio, and metallicity [C/H] derived from KPIC spectra of PDS 70b using the `petitRADTRANS` retrieval framework. See Section 5 for details.

$(0.28^{+0.20}_{-0.12})$ is consistent with the host star (0.44 ± 0.19; A. J. Cridland et al. 2023), and we find $\sim$ stellar metallicity. The high outer gas disk C/O value of $\gtrsim$1 measured by ALMA (S. Facchini et al. 2021; A. J. Cridland et al. 2023) and the PDS 70b values suggest that only a small fraction of carbon in the gas phase was and is within PDS 70b's Hill radius and that most of the carbon incorporated into PDS 70b arrived via ice and dust aggregates/solids.

In scenarios where the gas-phase carbon and oxygen are highly depleted in the outer disk, a small amount of accretion of solids onto PDS 70b can overwhelm the C/O contribution from the gas. Such gas-phase depletion, especially of CO, has been reported in other protoplanetary disks (e.g., TW Hya, DM Tau, IM Lup) and can be explained by chemical reactions or physical processes such as vertical mixing, freezing out onto dust grain, and radial drift. Thus, such depletion can be both radially dependent and time variable (C. Favre et al. 2013; K. Zhang et al. 2019; T. C. Yoshida et al. 2022), as exemplified by disks that do not exhibit CO depletion such as HD 163296 (K. Zhang et al. 2019) or many of the objects studied in an ALMA disk survey of the Lupus star-forming region (I. Pascucci et al. 2023).

A more accurate interpretation of the C/O in exoplanet atmospheres requires modeling of disk evolution, specifically the potentially divergent paths followed by dust/ice versus gas. One such model, by A. J. Cridland et al. (2023), provides an interpretation of our measured C/O and metallicity patterns in which the stellar-like C/O of PDS 70b is explained by late-stage carbon enrichment of the disk gas *after* the planet was formed. This model tracks the core accretion of volatile and refractory C, O species accretions onto the growing PDS 70b and c planets and simulates the concurrent evolution of the gas-phase chemistry in the disk, focusing on ^{12}CO, C^{18}O, and C_2H to track the C/O evolution. The authors find that the C/O values of the planets depend on the time when the disk was enriched with carbon through chemical or physical processes. If carbon is enriched throughout the disk lifetime, the planets would present a superstellar C/O ratio. Alternatively, if the disk carbon enrichment occurred relatively recently—after the planet was formed—PDS 70b will instead show a C/O value similar to its host star, consistent with our measurements. While not considered in the model above, photochemistry that sublimes and thus removes carbon in the pebbles during the planet's runaway gas accretion could also contribute to the observed lower C/O of the planet and the local C/O enhancement in the gas disk (H. Jiang et al 2023).

Growing evidence for the substantial evolution of the volatile element chemistry in the warm, inner region of disks has come from JWST (T. Henning et al. 2024; K. M. Pontoppidan et al. 2024). Thought to be driven by divergent dust+ice versus gas evolution, and first hinted at by Spitzer, JWST/MIRI spectra in particular reveal disk gas evolution from O-enriched at young (up to few Myr) ages (A. Banzatti et al. 2023, 2024; C. E. Muñoz-Romero et al. 2024) into a carbon-rich phase (I. Pascucci et al. 2013; B. Tabone et al. 2023; A. M. Arabhavi et al. 2024), especially in the disks around very low-mass stars. Recently, disks in possible transition between these phases have been found around Sun-like stars with low accretion rates, which display rich mixtures of water and complex carbonaceous species (M. J. Colmenares et al. 2024).

Placing the true nature of the formation history of PDS 70b into this general context will require more sophisticated disk modeling, ideally as a function of radius, along with our PDS 70b C/O measurement, to assess if the C/O of the gas at the location of PDS 70b is the same as the global C/O of the gas disk. In addition, the accretion history of PDS 70b, including the C/O of the dust and dust-to-gas ratio, should be considered more carefully in future modeling studies.

Observationally, we emphasize that our inferred parameters are based on our relatively noisy KPIC spectra (CO + H_2O CCF SNR ~ 4.2). Future observations of KPIC, VLT/CRIRES + (R. Follert et al. 2014), VLT/HiRISE (G. P. P. L. Otten et al. 2021), Subaru/REACH (T. Kotani et al. 2020), HISPEC (D. Mawet et al. 2019; Q. M. Konopacky et al. 2023), and

JWST/MIRI (M. Wells et al. 2015) will verify and improve our best estimates of the physical parameters of PDS 70b and possibly PDS 70c. While higher SNR measurements of C/O ratios will still be challenging to distinguish these two formation scenarios, the isotope ratios can be constrained to infer their accretion history of carbon and oxygen in the disk midplane, for example, $^{12}C/^{13}C$ and $^{16}O/^{18}O$ (Y. Zhang et al. 2021; J. W. Xuan et al. 2024a, 2024b), which requires very high CCF SNR > 50 for CO and H_2O main isotope species. Another way to disentangle the two scenarios from atmospheric characterizations of the planets is by measuring the refractory species such as Fe and Si in the near- (Fe H in J and H bands; M. C. Cushing et al. 2005) and mid-infrared (silicate clouds; G. Suárez & S. Metchev 2022; Y. Chachan et al 2023). On the other hand, a more accurate inference of PDS 70 planet formation history requires significant modeling work including tracing the volatile and refractory species and the associated isotopes for the planet and disk evolution in the future. Future discoveries and characterizations of more protoplanets for trends in the population of protoplanet compositions, with the next-generation telescopes such as the Giant Magellan Telescope, Thirty Meter Telescope, and Extremely Large Telescope, will allow us to statistically understand the formation and evolution of gas giant exoplanets at tens of astronomical units from their host stars.

7. Summary

In this Letter, we reported the detection and characterization of the super-Jovian protoplanet PDS 70b using Keck/KPIC high-resolution spectroscopy, with detections of atmospheric CO and H_2O.

Our detection of PDS 70b relies on a least-squares-based CCF, with the CCF SNRs for CO at 3.8σ, H_2O at 3.5σ, and CO and H_2O template at 4.2σ. We fit our KPIC spectra and derived a barycentric-corrected RV of PDS 70b ($\mathrm{RV} = -1.7^{+3.4}_{-5.2}$ km s^{-1}) different from its host star during the same epoch ($\mathrm{RV} = +6.65^{+0.14}_{-0.22}$ km s^{-1}), which is 2.5σ difference. We found the PDS 70b is consistent with the nondetection of the spin $v \sin i < 29$ km s^{-1} at 95% confidence level), which is expected given its ongoing accretion and contraction and its large radius ($2.7^{+0.4}_{-0.3}$ $R_{\rm Jup}$; J. J. Wang et al. 2020). We further validated our detection by comparing the star-only fit with our star and planet model and found that the star-only fit is highly disfavored by χ^2 ($\Delta\chi^2 = 772$) and the Bayes factor ($\log_{10}$Bayes factor $= 344.9$) statistics. Our atmospheric retrievals constrained the $\mathrm{C/O} = 0.28^{+0.20}_{-0.12}$ ($\lesssim$0.63 at 95% confidence level) and $[\mathrm{C/H}] = -0.2^{+0.8}_{-0.5}$ dex for PDS 70b.

Our measured C/O and metallicity of PDS 70b are consistent with those of the host star PDS 70 A (CO ~ 0.44; $[\mathrm{Fe/H}] = -0.11 \pm 0.19$ dex) and lower than the gas-phase C/O of the PDS 70 outer disk ($\gtrsim$1). The stellar-like C/O of PDS 70b can be interpreted via two scenarios. PDS 70b might have accreted the bulk materials of its carbon and oxygen from solids (dust+ice) instead of gas-phase volatiles, or PDS 70b might have formed before the disk gas was enriched in carbon. These scenarios cannot be distinguished by the existing C/O measurements of the star, planet, and its disk due to missing information on the accretion history of the planet PDS 70b, the dust C/O ratio, and the time-dependent dust-to-gas ratio. Future observations, with higher SNRs of PDS 70b and possibly PDS 70c for both volatile and refractory species, are required to refine and validate the true chemistry in their atmospheres, as well as a more detailed modeling of the whole system.

Acknowledgments

The authors thank Yayaati Chachan, Stefano Facchini, and Bruce Macintosh for extremely useful discussions on the physical interpretation of planet and disk chemistry, which have significantly improved this manuscript. The authors thank the anonymous referee for useful comments, which improved the original manuscript. The authors thank the Keck observing assistant Arina Rostopchina for her help in obtaining the Keck/KPIC spectra. W. M. Keck Observatory access was supported by Northwestern University and the Center for Interdisciplinary Exploration and Research in Astrophysics (CIERA). This research was supported in part through the computational resources and staff contributions provided for the Quest high-performance computing facility at Northwestern University which is jointly supported by the Office of the Provost, the Office for Research, and Northwestern University Information Technology. This work used computing resources provided by Northwestern University and the Center for Interdisciplinary Exploration and Research in Astrophysics (CIERA). Funding for KPIC has been provided by the California Institute of Technology, the Jet Propulsion Laboratory, the Heising-Simons Foundation (grant #2015-129, #2017-318, #2019-1312, and #2023-4598), the Simons Foundation (through the Caltech Center for Comparative Planetary Evolution), and the NSF under grant AST-1611623. This research has made use of the NASA Exoplanet Archive, which is operated by the California Institute of Technology, under contract with the National Aeronautics and Space Administration under the Exoplanet Exploration Program. Data presented herein were obtained at the W. M. Keck Observatory, which is operated as a scientific partnership among the California Institute of Technology, the University of California, and the National Aeronautics and Space Administration. The Observatory was made possible by the generous financial support of the W. M. Keck Foundation. The authors recognize and acknowledge the significant cultural role and reverence that the summit of Maunakea has with the indigenous Hawaiian community, and that the W. M. Keck Observatory stands on Crown and Government Lands that the State of Hawai'i is obligated to protect and preserve for future generations of indigenous Hawaiians.

Facilities: Keck:II (KPIC), Keck:II (NIRSPEC), Keck:II (NIRC2).

Software: `Astropy` (Astropy Collaboration et al. 2013, 2018), `DYNESTY` (J. S. Speagle 2020), `corner` (D. Foreman-Mackey 2016), `emcee` (D. Foreman-Mackey et al. 2013), `Matplotlib` (J. D. Hunter 2007), `Numpy` (C. R. Harris et al. 2020), `petitRADTRANS` (P. Molliére et al. 2019), `Scipy` (P. Virtanen et al. 2020), `seaborn` (M. L. Waskom 2021), `SMART` (C.-C. Hsu et al. 2021a, 2021b).

ORCID iDs

Chih-Chun Hsu https://orcid.org/0000-0002-5370-7494
Jason J. Wang (王劲飞) https://orcid.org/0000-0003-0774-6502
Geoffrey A. Blake https://orcid.org/0000-0003-0787-1610
Jerry W. Xuan https://orcid.org/0000-0002-6618-1137

Yapeng Zhang https://orcid.org/0000-0003-0097-4414
Jean-Baptiste Ruffio https://orcid.org/0000-0003-2233-4821
Katelyn Horstman https://orcid.org/0000-0001-9708-8667
Julianne Cronin https://orcid.org/0000-0003-1172-5755
Ben Sappey https://orcid.org/0000-0003-1399-3593
Yinzi Xin https://orcid.org/0000-0002-6171-9081
Luke Finnerty https://orcid.org/0000-0002-1392-0768
Daniel Echeverri https://orcid.org/0000-0002-1583-2040
Dimitri Mawet https://orcid.org/0000-0002-8895-4735
Nemanja Jovanovic https://orcid.org/0000-0001-5213-6207
Clarissa R. Do Ó https://orcid.org/0000-0001-5173-2947
Ashley Baker https://orcid.org/0000-0002-6525-7013
Benjamin Calvin https://orcid.org/0000-0003-4737-5486
Jacques-Robert Delorme https://orcid.org/0000-0001-8953-1008
Michael P. Fitzgerald https://orcid.org/0000-0002-0176-8973
Joshua Liberman https://orcid.org/0000-0002-4934-3042
Ronald A. López https://orcid.org/0000-0002-2019-4995
Evan Morris https://orcid.org/0000-0003-3165-0922
Andrew Skemer https://orcid.org/0000-0001-6098-3924
J. Kent Wallace https://orcid.org/0000-0001-5299-6899
Ji Wang (王吉) https://orcid.org/0000-0002-4361-8885

References

Arabhavi, A. M., Kamp, I., Henning, T., et al. 2024, Sci, 384, 1086
Astropy Collaboration, Price-Whelan, A. M., Sipőcz, B. M., et al. 2018, AJ, 156, 123
Astropy Collaboration, Robitaille, T. P., Tollerud, E. J., et al. 2013, A&A, 558, A33
Banzatti, A., Pontoppidan, K. M., Carr, J. S., et al. 2023, ApJL, 957, L22
Banzatti, A., Salyk, C., Pontoppidan, K. M., et al. 2024, arXiv:2409.16255
Baraffe, I., Homeier, D., Allard, F., & Chabrier, G. 2015, A&A, 577, A42
Benneke, B., & Seager, S. 2013, ApJ, 778, 153
Bowler, B. P. 2016, PASP, 128, 102001
Bowler, B. P., Tran, Q. H., Zhang, Z., et al. 2023, AJ, 165, 164
Bryan, M. L., Ginzburg, S., Chiang, E., et al. 2020, ApJ, 905, 37
Cale, B., Plavchan, P., LeBrun, D., et al. 2019, AJ, 158, 170
Chachan, Y., Knutson, H. A., Lothringer, J., & Blake, G. A. 2023, ApJ, 943, 112
Chan, Y. M., & Dalgarno, A. 1965, PPS, 85, 227
Christiaens, V., Casassus, S., Absil, O., et al. 2019, MNRAS, 486, 5819
Colmenares, M. J., Bergin, E., Salyk, C., et al. 2024, arXiv:2410.18187
Cowley, A., Cowley, C., Jaschek, M., & Jaschek, C. AJ 1969, 74, 375
Cridland, A. J., Facchini, S., van Dishoeck, E. F., & Benisty, M. 2023, A&A, 674, A211
Cugno, G., Patapis, P., Stolker, T., et al. 2021, A&A, 653, A12
Currie, T., Biller, B., Lagrange, A., et al. 2023, in ASP Conf. Ser. 534, Protostars and Planets VII, ed. S. Inutsuka et al. (San Francisco, CA: ASP), 799
Currie, T., Lawson, K., Schneider, G., et al. 2022, NatAs, 6, 751
Cushing, M. C., Rayner, J. T., & Vacca, W. D. 2005, ApJ, 623, 1115
Cutri, R. M., Skrutskie, M. F., van Dyk, S., et al. 2003, yCat, II/246,
Dalgarno, A., & Williams, D. A. 1962, ApJ, 136, 690
Delorme, J.-R., Jovanovic, N., Echeverri, D., et al. 2021, JATIS, 7, 035006
Echeverri, D., Jovanovic, N., Delorme, J.-R., et al. 2024, Proc SPIE, 13096, 130962D
Facchini, S., Teague, R., Bae, J., et al. 2021, AJ, 162, 99
Favre, C., Cleeves, L. I., Bergin, E. A., Qi, C., & Blake, G. A. 2013, ApJL, 776, L38
Follert, R., Dorn, R. J., Oliva, E., et al. 2014, Proc. SPIE, 9147, 914719
Foreman-Mackey, D. 2016, JOSS, 1, 24
Foreman-Mackey, D., Hogg, D. W., Lang, D., & Goodman, J. 2013, PASP, 125, 306
Gaia Collaboration, Brown, A. G. A., Vallenari, A., et al. 2018, A&A, 616, A1
Gaia Collaboration, Vallenari, A., Brown, A. G. A., et al. 2023, A&A, 674, A1
Gray, D. F. 2008, The Observation and Analysis of Stellar Photospheres (3rd; Cambridge: Cambridge Univ.Press),
Haffert, S. Y., Bohn, A. J., de Boer, J., et al. 2019, NatAs, 3, 749
Hargreaves, R. J., Gordon, I. E., Rey, M., et al. 2020, ApJS, 247, 55
Harris, C. R., Millman, K. J., van der Walt, S. J., et al. 2020, Natur, 585, 357
Hashimoto, J., Aoyama, Y., Konishi, M., et al. 2020, AJ, 159, 222
Henning, T., Kamp, I., Samland, M., et al. 2024, PASP, 136, 054302
Horne, K. 1986, PASP, 98, 609
Horstman, K. A., Ruffio, J.-B., Wang, J. J., et al. 2024, Proc. SPIE, 13096, 130962E
Hsu, C.-C., Burgasser, A. J., Theissen, C. A., et al. 2021a, ApJS, 257, 45
Hsu, C.-C., Burgasser, A. J., & Theissen, C. A. 2023, ApJL, 945, L6
Hsu, C.-C., Burgasser, A. J., Theissen, C. A., et al. 2024a, ApJS, 274, 40
Hsu, C.-C., Theissen, C., Burgasser, A., & Birky, J. 2021b, SMART: The Spectral Modeling Analysis and RV Tool, v1.0.0, Zenodo, doi:10.5281/zenodo.4765258
Hsu, C.-C., Wang, J. J., Xuan, J. W., et al. 2024b, ApJ, 971, 9
Hunter, J. D. 2007, CSE, 9, 90
Jeffreys, H. 1961, Theory of Probability (3rd ed.; Oxford: Oxford Univ. Press)
Jiang, H., Wang, Y., Ormel, C. W., Krijt, S., & Dong, R. 2023, A&A, 678, A33
Keenan, P. C. 1993, PASP, 105, 905
Keppler, M., Benisty, M., Müller, A., et al. 2018, A&A, 617, A44
Konopacky, Q. M., Baker, A. D., Mawet, D., et al. 2023, Proc. SPIE, 12680, 1268007
Kotani, T., Kawahara, H., Ishizuka, M., et al. 2020, Proc. SPIE, 11448, 1144878
Law, C. J., Benisty, M., Facchini, S., et al. 2024, ApJ, 964, 190
Marley, M., Saumon, D., Morley, C., & Fortney, J. 2018, Sonora 2018: Cloud-free, Solar Composition, Solar C/O Substellar Evolution Models, v1.0, Zenodo, doi:10.5281/zenodo.2628068
Marley, M. S., Saumon, D., Visscher, C., et al. 2021, ApJ, 920, 85
Martin, E. C., Fitzgerald, M. P., McLean, I. S., et al. 2018, Proc. SPIE, 10702, 107020A
Mawet, D., Delorme, J. R., Jovanovic, N., et al. 2017, Proc. SPIE, 10400, 1040029
Mawet, D., Fitzgerald, M., Konopacky, Q., et al. 2019, BAAS, 51, 134
Mawet, D., Wizinowich, P., Dekany, R., et al. 2016, Proc. SPIE, 9909, 99090D
Mayor, M., & Queloz, D. 1995, Natur, 378, 355
McLean, I. S., Becklin, E. E., Bendiksen, O., et al. 1998, Proc. SPIE, 3354, 566
McLean, I. S., Graham, J. R., Becklin, E. E., et al. 2000, Proc. SPIE, 4008, 1048
Moehler, S., Modigliani, A., Freudling, W., et al. 2014, A&A, 568, A9
Mollière, P., Stolker, T., Lacour, S., et al. 2020, A&A, 640, A131
Molliére, P., Wardenier, J. P., van Boekel, R., et al. 2019, A&A, 627, A67
Muñoz-Romero, C. E., Banzatti, A., Öberg, K. I., et al. 2024, ApJ, 975, 78
Müller, A., Keppler, M., Henning, T., et al. 2018, A&A, 617, L2
Öberg, K. I., Murray-Clay, R., & Bergin, E. A. 2011, ApJL, 743, L16
Otten, G. P. P. L., Vigan, A., Muslimov, E., et al. 2021, A&A, 646, A150
Pascucci, I., Herczeg, G., Carr, J. S., & Bruderer, S. 2013, ApJ, 779, 178
Pascucci, I., Skinner, B. N., Deng, D., et al. 2023, ApJ, 953, 183
Pecaut, M. J., & Mamajek, E. E. 2016, MNRAS, 461, 794
Perotti, G., Christiaens, V., Henning, T., et al. 2023, Natur, 620, 516
Pfalzner, S., & Dincer, F. 2024, ApJ, 963, 122
Pontoppidan, K. M., Salyk, C., Banzatti, A., et al. 2024, ApJ, 963, 158
Ratzenböck, S., Großschedl, J. E., Alves, J., et al. 2023a, A&A, 678, A71
Ratzenböck, S., Großschedl, J. E., Möller, T., et al. 2023b, A&A, 677, A59
Riaud, P., Mawet, D., Absil, O., et al. 2006, A&A, 458, 317
Rothman, L. S., Gordon, I. E., Barber, R. J., et al. 2010, JQSRT, 111, 2139
Ruffio, J.-B., Horstman, K., Mawet, D., et al. 2023, AJ, 165, 113
Speagle, J. S. 2020, MNRAS, 493, 3132
Steinmetz, M., Guiglion, G., McMillan, P. J., et al. 2020a, AJ, 160, 83
Steinmetz, M., Matijevič, G., Enke, H., et al. 2020b, AJ, 160, 82
Suárez, G., & Metchev, S. 2022, MNRAS, 513, 5701
Swastik, C., Banyal, R. K., Narang, M., et al. 2021, AJ, 161, 114
Tabone, B., Bettoni, G., van Dishoeck, E. F., et al. 2023, NatAs, 7, 805
Thanathibodee, T., Molina, B., Calvet, N., et al. 2020, ApJ, 892, 81
Theissen, C. A., Konopacky, Q. M., Lu, J. R., et al. 2022, ApJ, 926, 141
Virtanen, P., Gommers, R., Oliphant, T. E., et al. 2020, NatMe, 17, 261
Wang, J. J., Ginzburg, S., Ren, B., et al. 2020, AJ, 159, 263
Wang, J. J., Kulikauskas, M., & Blunt, S., 2021a whereistheplanet: Predicting Positions of Directly Imaged Companions, Astrophysics Source Code Library, ascl:2101.003
Wang, J. J., Ruffio, J.-B., Morris, E., et al. 2021b, AJ, 162, 148

Wang, J. J., Vigan, A., Lacour, S., et al. 2021c, AJ, 161, 148
Waskom, M. L. 2021, JOSS, 6, 3021
Wells, M., Pel, J. W., Glasse, A., et al. 2015, PASP, 127, 646
Xuan, J. W., Hsu, C.-C., Finnerty, L., et al. 2024a, ApJ, 970, 71
Xuan, J. W., Wang, J., Finnerty, L., et al. 2024b, ApJ, 962, 10
Xuan, J. W., Wang, J., Ruffio, J.-B., et al. 2022, ApJ, 937, 54
Yoshida, T. C., Nomura, H., Tsukagoshi, T., Furuya, K., & Ueda, T. 2022, ApJL, 937, L14
Zhang, K., Bergin, E. A., Schwarz, K., Krijt, S., & Ciesla, F. 2019, ApJ, 883, 98
Zhang, Y., Snellen, I. A. G., Bohn, A. J., et al. 2021, Natur, 595 370